Statistical and Temporal Characteristics of Sawtooth Events

Connor C. DiMarco[1,2], Tuija I. Pulkkinen[1], and Michael G. Henderson[2]

[1]University of Michigan, Ann Arbor, MI, USA
[2]Los Alamos National Laboratory, Los Alamos, NM, USA

Correspondence: Connor C. DiMarco (cdimarco@umich.edu)

Abstract. Magnetospheric sawtooth events are characterized by periodic particle injections and magnetic dipolarizations spread quasi-simultaneously across a wide range of magnetic local times. We present a comprehensive statistical study of magnetospheric sawtooth events (STEs) during solar cycle 24 (2008–2016), extending previous catalogs and enabling solar cycle comparisons. Our results confirm that STEs predominantly occur during the ~~declining phase~~ rising and declining phases

5   of the solar cycle, and are strongly associated with geomagnetic storms. Superposed epoch analysis reveals near-simultaneous particle injections across all magnetic local time sectors, but magnetic field dipolarization confined to the midnight region~~, supporting~~. These results support a scenario in which nightside tail reconnection and enhanced convection are the primary drivers of sawtooth oscillations. The localization of magnetic dipolarizations during STEs challenges global instability interpretations and suggest that STEs represent a stormtime substorm mode triggered under specific solar wind and magnetotail

10   conditions. Superposed epoch analyses also show enhanced oxygen content in the magnetosphere during sawtooth events, but do not show a significant difference from geomagnetic storms that do not exhibit periodic behavior.

1 Introduction

Magnetospheric ~~Sawtooth~~ active periods organize into operational modes: substorms, steady convection, sawteeth, and storms, ordered by increasing intensity and distinct system-scale responses. Substorms are tail reconfigurations marked by energetic

15   particle injections and inner-magnetosphere dipolarization, plasmoid release from the tail, and enhancement of the westward electrojet (Baker et al., 1996; Angelopoulos et al., 2009). Steady convection intervals are periods of enhanced solar-wind driving without discrete substorm expansions, with elevated but smoothly varying ionospheric currents and continuous elevated AL activity (Sergeev et al., 1996; Partamies et al., 2009). Storms reflect strong ring-current enhancement under sustained driving (Gonzalez et al., 1994; Kilpua et al., 2017b). Sawtooth events consist of quasi-periodic energetic particle injections spanning

20   broad local-time sectors, often embedded within storm intervals and exhibiting repeatable magnetospheric cycling (Henderson et al., 2006; ? . Determining why the magnetosphere-ionosphere system responds by one mode versus another is a core space physics problem with unknown thresholds and control parameters. Furthermore, whether these categories represent a continuum of responses to external driving, or invoke distinct internal physics, remains unresolved. The answer carries weight because each mode couples differently to the ionosphere and inner magnetosphere, altering storm-time space weather hazards and forecasting requirements

25   (Baker et al., 2013).

Magnetospheric Sawtooth Events (STEs) have been described as periodic particle injections accompanied by magnetic dipolarizations, primarily observed from geostationary orbit (Henderson et al., 2006). While a strict definition of a sawtooth event does not exist, they are commonly identified by their qualitative features (see Figure 1 for a sample event). The top panel shows proton fluxes integrated over a broad energy range (50-400 keV) from three Los Alamos National Laboratory (LANL) energetic particle detectors onboard spacecraft that were approximately 120 degrees apart – indicating quasi-simultaneous energetic particle injections around the globe. Vertical dashed lines marking successive tooth onsets across geosynchronous observations with LANL proton fluxes show that GOES-10 (in the night sector in the shaded region, 21-3 MLT) B_z exhibits step-like dipolarizations at the times of the tooth onset. The figure also shows the upstream IMF B_z and solar-wind V_x as well as the AU/AL and SYM-H indices, which reveal the high geomagnetic activity in the ionosphere and strong upstream driving conditions for context.

While several authors have addressed the characteristics and drivers of sawtooth oscillations (Henderson et al., 2006; Pulkkinen et al., 2007; Cai and Clauer, 2009; Fung et al., 2016), there are still major disagreements in the definition of a sawtooth event as the physical processes that drive these phenomena, leading to several different theories to describe STE formation.

Lee (2004) suggests that sawtooth oscillations are driven by solar wind and interplanetary magnetic field (IMF) fluctuations. They demonstrated that periodic behavior at geosynchronous orbit can be associated with periodic solar wind pressure pulses driving either periodic compressions or substorms in the magnetosphere. However, we note that as shown by Lee et al. (2006), there are sawtooth events that are not associated with periodic solar wind driving. Therefore, even if there is a periodic driver, there are other conditions that lead to similar periodic behavior.

Furthermore, several scenarios have been employed for producing periodic global (from nightside to dayside) stretching and dipolarization of the inner magnetosphere magnetic field. First, the dayside stretching has been associated with an increased plasma pressure and current in the dayside magnetosphere, created by strong convection from the nightside plasma sheet (Pulkkinen et al., 2006). Second, global stretching has been suggested to arise from increased pressure from the lobe magnetic field: as the cusps move sunward under polar-cap potential saturation, magnetic pressure from the northern and southern lobes on the dayside closed magnetosphere increases (Borovsky et al., 2009). Third, the dayside stretching has been associated with strong Region-1 current under polar cap saturation conditions, weakening the dipole magnetic field in the dayside equatorial magnetosphere (Borovsky et al., 2009).

Prior studies have also associated ionospheric outflow as an active driver of STE-like periodicity via mass loading of the magnetotail (Brambles et al., 2011). Heavy ions can lower effective Alfvén speeds and modulate the reconnection inflow, establishing a loading–unloading cycle that recurs at outflow periodicity. In global simulations, outflow-driven pressure builds until a threshold is reached, triggering plasmoid release and dipolarization before the system resets; the recurrence time scales

with magnetosphere–ionosphere coupling strength and outflow occurrence (Brambles et al., 2011). Event-based and modeling analyses further indicate that outflow effects are especially consequential under sustained moderate driving (e.g., stream interaction regions or steady southward IMF), whereas strong transient drivers (ICMEs) can also produce sawtooth-like cycling with weaker outflow requirements, implying multiple pathways to STE phenomenology (Brambles et al., 2013). Observational studies show some differences in O^+ and H^+ outflow between storms with and without sawteeth suggesting a link between outflow and sawtooth occurrence, but it is unclear whether enhanced oxygen in the magnetosphere is critical for sawtooth storm development (Nowrouzi et al., 2024). Finally, global MHD-kinetic simulations have demonstrated that sawtooth oscillations can arise under strong, steady driving without enhanced ionospheric outflow, with magnetotail kinetic reconnection determining the loading–unloading cycle (Wang et al., 2022). Together these results suggest that ionospheric outflow may modulate thresholds, cadence, and composition, but are not strictly necessary to produce STE-like oscillations. Likewise, they suggest that sawtooth oscillations may emerge from reconnection-driven magnetotail dynamics under suitable upstream conditions.

Lastly, it has been argued that the sawtooth injections are driven by the same mechanisms as substorms, and that periodic substorms and sawtooth events represent a continuum from weaker to stronger driving ~~(?Henderson, 2016)~~(Pulkkinen et al., 2007; Henderson, . Although in some events the dispersionless injections have been observed to reach all the way into the dayside geostationary orbit (Borovsky et al., 2004), it has been shown that in some cases these injections are in fact not fully dispersionless (Henderson et al., 2006), but only appear to be so due to the high drift speed during strong convection. Examination of the full energy spectrum including the lower energy plasma shows that these injections indeed are not completely dispersionless, but originate from the magnetotail where the dispersion signatures are smallest. This would suggest that sawtooth events might ~~be~~ form a class of substorms with ~~strong enough~~ sufficiently strong convection to exhibit global quasi-dispersionless energetic particle injections.

~~Prior statistical STE studies (Fung et al., 2016) all focus on time period prior to 2007. Here we return to the physics of sawtooth events by creating a comprehensive list~~ This study compiles a Solar Cycle 24 catalog of sawtooth events ~~covering a full solar cycle (2008-2018), while comparing and complementing these observations with the prior studies focusing on the previous solar cycle. For the first time, we also analyze the magnetic field stretching and dipolarization in a statistical sense~~(2008–2016), extending the pre-2008 datasets to enable cycle-to-cycle comparison of occurrence, intertooth cadence, and teeth counts. Using energetic particle data from the Los Alamos Geostationary Satellites and GOES magnetometers with superposed-epoch analysis resolved by magnetic local time, the work quantifies injection simultaneity versus magnetic-field dipolarization to diagnose the geometry and sectoral confinement of reconfiguration. The approach tests global-instability expectations against a reconnection-and-convection scenario by contrasting near-simultaneous injections at all MLTs with the localization of dipolarization to midnight. The results provide a geostationary, mode-aware baseline for interpreting stormtime variability and clarify how sawtooth events relate to substorms under strong driving.
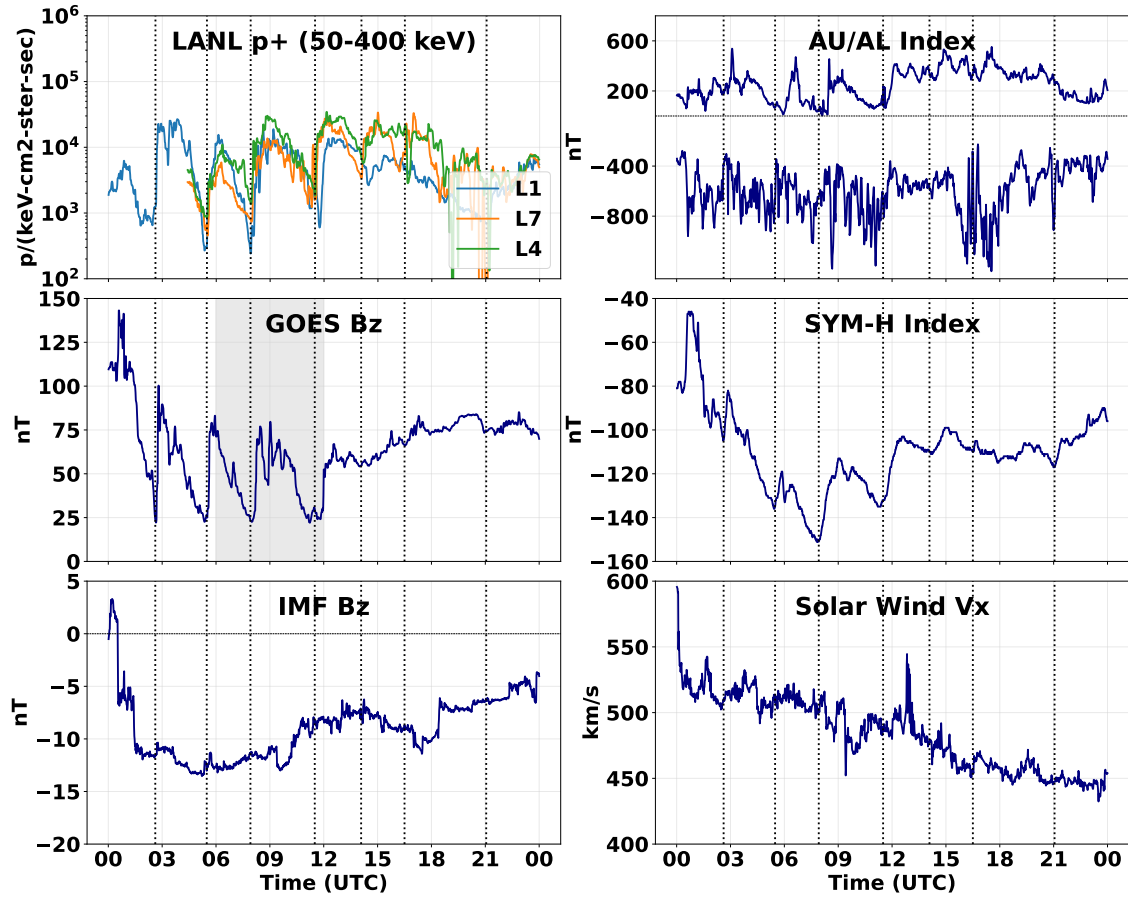
2   Data

Figure 1. An example of a sawtooth event during April 18, 2002. Left: (~~left~~top) Geosynchronous orbit ion fluxes ~~and Bz, from~~ the Los Alamos geostationary satellites the LANL energetic particle instruments. (middle) $B_{z,GSM}$ from GOES-10. (bottom) IMF B_z from the OMNI database. Right: (top) AU~~and /~~AL ~~indices~~Indices, ~~and the~~ (middle) SYM-H ~~index during the April 18th 2002 sawtooth event.~~ Index, and (~~right~~bottom) ~~Possible magnetic field change scenario associated with~~ solar wind speed from the OMNI database. The sawtooth ~~events~~onsets are indicated with vertical dashed lines.

Our study covers an eight-year period from 2008 to 2016, during which there were between 3 and 6 LANL energetic particle instruments onboard spacecraft at varying longitudes at geostationary orbit.

95   Identification of sawtooth injections was done using the Los Alamos National Laboratory (LANL) ~~GEOGRID~~ GeoGrid data. The low-energy particle detector is designed to measure key plasma parameters such as density, temperature, and bulk velocity

of ions and electrons at geosynchronous orbit (Bame et al., 1993). The instrument covers the low-energy plasma populations in the range ~~of~~ from a few eV to several keV, providing insights into the dynamics of the background plasma environment during magnetospheric disturbances, and into dispersion patterns of the particle injections. The high-energy particle instrument

100 measures ~~the flux~~ fluxes of energetic ions and electrons in the range ~~of~~ from tens of keV to several MeV (Belian et al., 1992). The instrument is particularly ~~suited~~ well-suited for detecting energetic particle injections and enhancements during geomagnetic storms, substorms, and sawtooth events. We use the high-energy proton observations to identify sawtooth events, searching for periodic particle injections. The "sawtooth" signature is characterized by periodic sharp flux increases followed by slow decreases, observed simultaneously by ~~the multiple spacecraft placed~~ multiple spacecraft located across a broad range

105 of local times. ~~Our study covers a 10-year period from 2008 to 2018, during which there are between 3 and 6 satellites available at varying longitudes of the geostationary orbit.~~

The ~~vertical lines in Figure 1 show the start of the sudden increases of the fluxes, which we identify as the onset of the sawtooth injection.~~

~~The~~ magnetic field dipolarizations during the sawtooth events ~~can be observed in the magnetometer observations from the~~

110 ~~two geostationary orbit spacecraft~~ are recorded using data from the magnetic field instruments onboard the two Geostationary Operational Environmental Satellites (GOES) located above the eastern and western ~~US (Singer et al., 1996).~~ United States at any given time (Singer et al., 1996). For the time period 2008-2016, the spacecraft in orbit varied. Data was aggregated from GOES 10, 11, 12, 13, 14, and 15. Furthermore, for added longitudinal coverage, we use the field inclination deduced from the energetic particle distribution functions (Thomsen et al., 1996; Chen et al., 2016).

115 ## 3 ~~Methodology~~

Magnetospheric oxygen content is processed from the Van Allen Probes' Helium, Oxygen, Proton, and Electron (HOPE) mass spectrometers (Spence et al., 2013). The RBSP-ECT HOPE mass spectrometers provide composition-resolved electrons and ions (H^+, He^+, O^+) from roughly the greater of spacecraft potential or $\sim$20 eV up to $\sim$45 keV, using an electrostatic top-hat analyzer with time-of-flight coincidence to reject penetrating backgrounds and to separate species unambiguously

120 (Funsten et al., 2013). HOPE returns pitch-angle–resolved differential fluxes at spin cadence and enables derivation of species moments (density, temperature, partial pressure), allowing direct quantification of stormtime O^+ loading, O^+/H^+ ratios, and O^+ partial pressures across onset and recovery. In this work, HOPE measurements are used to test whether O^+ enhancements precede or accompany injections and to quantify O^+ contributions.

Solar wind, IMF, and geomagnetic index context were obtained from NASA's OMNI database at the Space Physics Data

125 Facility (SPDF, NASA Goddard Space Flight Center, 2025). OMNI provides upstream speed, density, and dynamic pressure at high-resolution and time-shifted to the bow-shock nose. The SYM-H and AL indices are used to characterize storm-time evolution and to provide context for sawtooth intervals.

3 Identification of Sawtooth Events

We compiled a list of sawtooth injections by visual inspection of the LANL proton flux data in the energy range from 100 to
500 keV. The energetic particle data was then combined with the SYM-H index from the OMNI database (Papitashvili et al.,
2014) and magnetic field from the GOES spacecraft (Singer et al., 1996). For each event, we identified individual tooth onset
times, with the tooth onset defined as the earliest time of the injection across the available ~~spacecraft. It is important to note
that this list was created using a qualitative process (visual identification), and may not include all of the sawtooth events that
may have occurred during this time interval.~~ LANL observations. The list of sawtooth events containing 81 events is provided
in the Supplement~~(supplement.pdf).~~.

We compare our results with a previous list of sawtooth events published by Cai and Clauer (2009), here referred to as CC09,
that covers much of Solar Cycle 23 with a total of 111 sawtooth intervals containing 438 separate teeth. ~~This study utilized a
similar method of event identification; together~~ Together, the two lists cover almost two full solar cycles. Figure 2 shows the
occurrence of sawtooth events in relation to the solar cycle, spanning 18 years of observations. The number of sawtooth events
per year are shown with data from CC09 in blue and this study in red. Overlaid in gray is the yearly sunspot number, which
provides a proxy for solar activity and solar cycle phase.

Both this catalog and CC09 were compiled in the same manner, by visual identification of LANL geostationary energetic
proton injections, adopting the earliest onset across the constellation as the tooth time. Thus, both lists share inherent subjectivity
in event discrimination. Accordingly, both catalogs should be regarded as lower bounds on STE occurrence, with likely
omissions concentrated in periods of incomplete local-time coverage, instrument gaps, or ambiguous morphology during
intense storms. A cross-check against CC09 shows similar annual occurrence patterns and comparable distributions of intertooth
intervals and teeth-per-event over overlapping solar-cycle phases, indicating catalog-level consistency despite independent
selection.

Sawtooth events show a strong positive correlation with the solar cycle, reinforcing the ~~idea~~ fact that the vast majority (95%)
occur during geomagnetic storms (Cai et al., 2011; Cai and Clauer, 2009). Interestingly, the occurrence of sawtooth events does
not peak precisely at solar maximum~~but rather during the declining phase of the solar cycle~~, but rather shows a minimum right
at the solar maximum – resembling the occurrence frequency of interplanetary coronal mass ejections (ICMEs) and magnetic
clouds ~~(?). For solar cycle 24, the vast majority of the events occur during geomagnetic storms.~~ that often peak during the
declining phase of the solar cycle (Kilpua et al., 2011). This may be indicative of the highly variable solar wind and IMF
conditions at solar maximum, which do not foster driving of long-duration periodic activity in the magnetosphere.

The bottom panels of Figure 2 present a comparative analysis of sawtooth event characteristics across the CC09 time period
and this study. The ~~top-left panel shows~~ left panels show the distribution of inter-tooth intervals, showing the time between two
successive onsets, while the ~~top-right panel shows~~ right panels show the number of teeth per sawtooth event. Both distributions
are presented for two datasets: the CC09 (blue) covering the period 1998–2008, and this study (red) covering the period 2008–
2016. The two plots below show the combined distributions of intertooth times and number of teeth per sawtooth event, as the
larger combined dataset better illustrates the statistical properties of sawtooth occurrence.
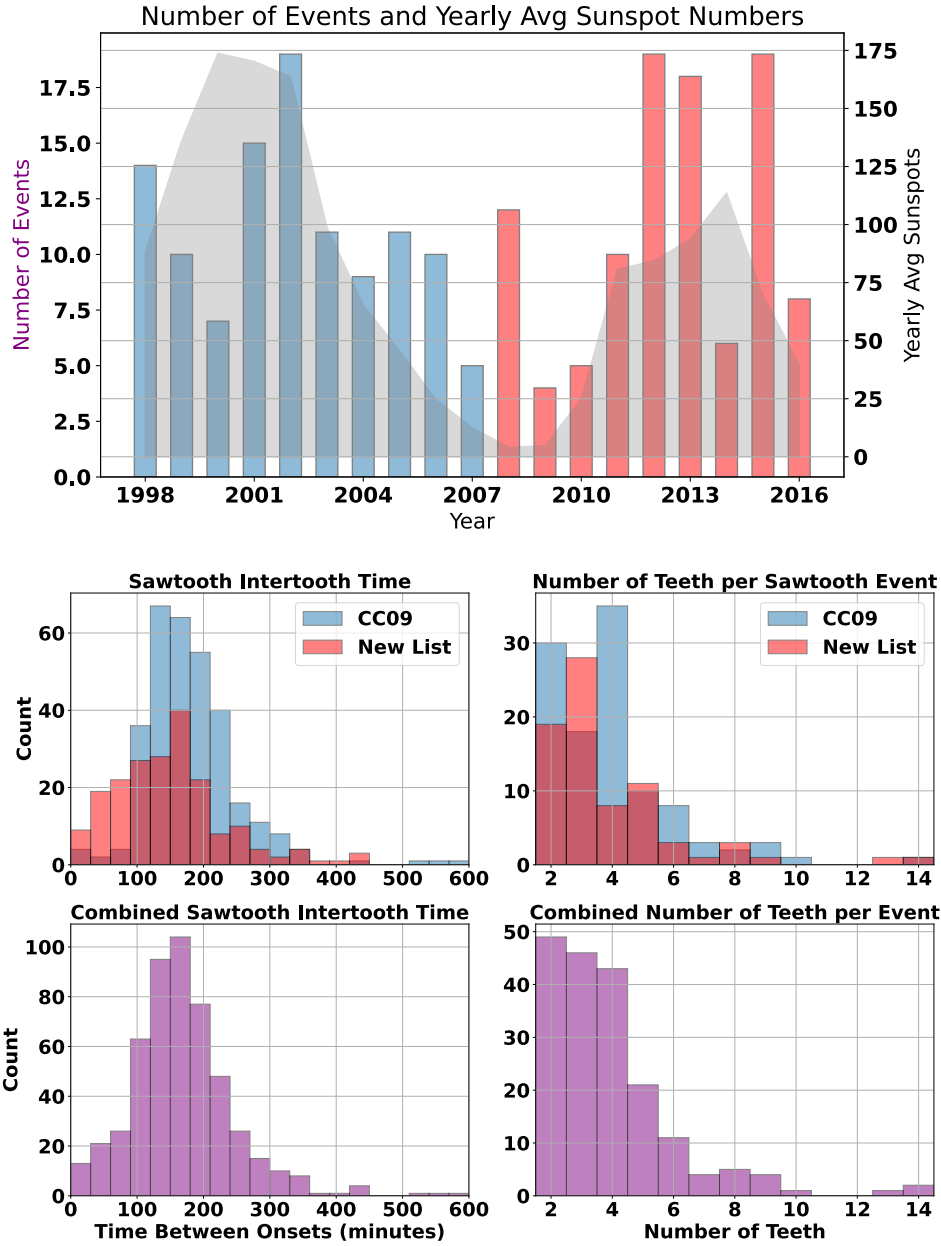
Figure 2. (top) Annual distribution of sawtooth event occurrence with the annual sunspot number on the background. (middle left) Average duration between two sawtooth injection onsets (intertooth interval) for this study (red) and CC09 (blue). (middle right) Average number of teeth per event for this study (red) and CC09 (blue). (bottom left) Combined average duration between sawtooth injections. (bottom right) Combined average number of teeth per event.

The inter-tooth interval distributions reveal that during both ~~periods~~solar cycles, most events occur within 400 minutes (∼7 hours) the highest concentration of intervals below 200 minutes. However, our dataset exhibits a slightly broader distribution, with a higher frequency of longer intervals, suggesting a higher variability in event spacing~~and a potential bias in event selection.~~. The distribution of teeth per sawtooth event shows that the majority of events contain 2-6 teeth, with a peak around 2–4 teeth. While both datasets exhibit similar overall trends, CC09 has a more pronounced peak at 4 teeth, whereas our events have a slightly wider spread, indicating more frequent occurrences of both ~~low- and high-teeth events , or another potential selection effect.~~ events with low and high number of teeth. The intertooth interval peak at 160 min is consistent with the ~~observed~~ previously reported recurrence period of substorms of 2–4 hours (Borovsky and Yakymenko, 2017) and very close to the value obtained by Freeman and Morley (2004) for substorm recurrence of 2.7 hours. Note that some of the differences in the distributions may arise from selection biases by the list curators.

4 ~~Results~~Sawtooth Signatures at Geostationary Orbit

Figure 3 shows a superposed epoch analysis (SEA) of sawtooth event signatures at geostationary orbit in four magnetic local time (MLT) quadrants (~~09-15 MLT, 15-21 MLT, 21-03~~ 09–15 MLT, 15–21 MLT, 21–03 MLT, and ~~03-09~~03–09 MLT). The SEA algorithm calculates the mean behavior of a given quantity around an epoch time (here the sawtooth injection onset time). The SEA was applied to the proton and electron fluxes using linear averaging of the actual flux values. Similarly, the SEA was applied to the magnetic field inclination angle derived from the GOES magnetometers and LANL distribution functions. Because of the different instrumentation ~~to calculate~~ used to derive the field inclination, we show the LANL and GOES magnetic field results separately.

The superposed epoch analysis shows a prompt increase of energetic proton and electron fluxes, with the nightside showing the first response, but the other three local time sectors showing rather similar enhancements after short delay times that don't significantly differ between electrons and protons. Furthermore, the average magnitude of the flux increase is about the same in each quadrant, indicating that roughly the same population reaches the geostationary orbit at all local times.

The magnetic field inclination is compared with the quiet time value taken to be the T89 model using $Kp = 2$ (Tsyganenko, 1989). Note that the data from geostationary satellites include a diurnal sinusoidal variability as even during quiet times, the magnetic field is more stretched (smaller inclination angle) in the nightside and more compressed (higher inclination angle) in the dayside. Thus, one would expect the dawn and dusk sectors to show decreasing and increasing tilt angles, respectively, as the spacecraft move eastward in their orbits, while the noon and midnight would show a maximum and minimum of the field, respectively, as the spacecraft move eastward across the noon-midnight meridian. The T89 model results clearly demonstrate this diurnal variation, and can be used as a "quiet-time baseline" for comparison.

In the midnight sector, the field is stretched, and stretches further during the hour prior to the onset. Following the injection, the field dipolarizes but does not reach the model field value, indicating that the tail and magnetospheric current systems have not completely reconfigured ~~(Baker et al., 1996)~~(Baker et al., 1996; Pulkkinen et al., 2007). The dawn and dusk fields, likewise, show a strongly stretched field, but only a minor field inclination change at the time of the injection. The dayside field
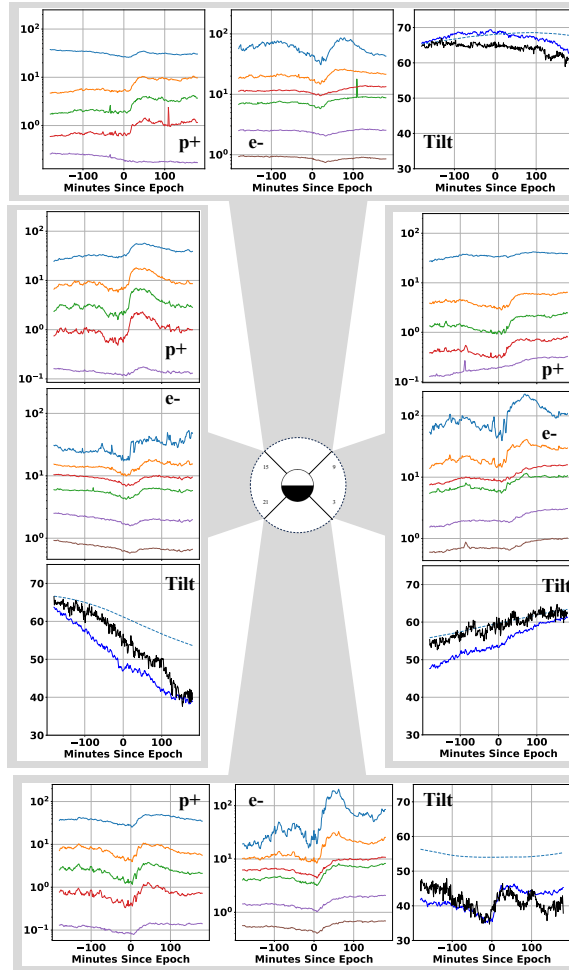
Figure 3. Superposed epoch analysis of ion and electron injections and magnetic field inclination angle carried out separately in four local time quadrants. The proton channels from the LANL SOPA instruments are 92, 138, 206, and 316 keV, and the electron channels are 125, 183, 266, 396, 612, and 908 keV (from top to bottom of each panel, respectively, as the flux values decrease with increasing energy). The field inclination panels show the results from aggregated GOES magnetometers (black) together with particle distribution function -based estimation from the LANL data (blue). The model magnetic field from Tsyganenko (1989) model for $Kp = 2$ (dashed line) is shown for reference.

195   is strongly compressed (more dipolar than model) prior to the injection, while the field is stretched following the arrival of the energetic particle population.

5   Drivers of Sawtooth Oscillations

Interplanetary Coronal Mass Ejections (ICME) and Stream Interaction Regions (SIR) are large-scale solar wind structures that exhibit distinct solar-cycle dependencies (Kilpua et al., 2017a; Heber et al., 1999; Hajra and Sunny, 2022). CME occurrence

200 peaks near sunspot maximum and remains elevated into the declining phase, whereas SIRs become increasingly prevalent through the declining phase and into solar minimum as long-lived coronal holes drive recurrent high-speed streams (Kilpua et al., 2017a, b; . Figure 2, which shows enhanced sawtooth occurrence at the rising and declining phases of the solar cycle, might suggest a relationship between CMEs and SIRs as solar wind drivers and STEs as their magnetospheric responses.

Figure 4 divides the sawtooth events into those occuring during ICME and SIR intervals, and to those that do not occur during

205 either ICMEs or SIRs. Here we show the total number of sawtooth onsets occurring in each driver category. The ICME periods were identified using the list assembled by (Richardson and Cane, 2010), while the SIRs list comes from (Grandin et al., 2019) . There are 331 sawteeth during ICME intervals, 300 sawteeth during SIR intervals, and 164 sawteeth in the "neither" category. This result is consistent with the solar-cycle variability shown in Figure 2, while the substantial number of events occurring during other than ICME/SIR intervals demonstrates that they are not the exclusive drivers of sawtooth oscillations. Furthermore,

210 it is unclear what drives the relatively high number of sawtooth oscillations in the rising phase of the solar cycle, when ICME-storms are less numerous than during corresponding activity in the declining phase (Kilpua et al., 2011).
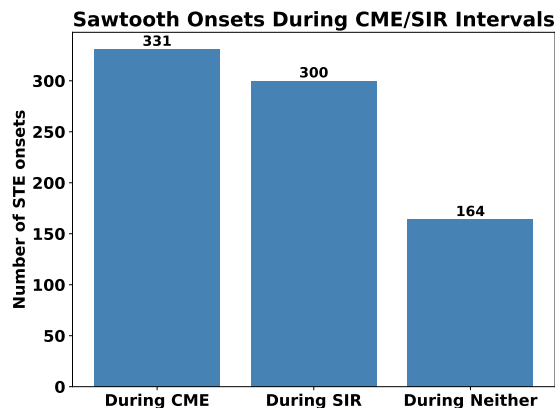

Figure 4. ~~Superposed epoch analysis~~ Bar chart of ~~ion and electron injections and magnetic field inclination angle carried out separately in four local time quadrants. The proton channels are 92~~sawtooth onsets occurring during ICME intervals, ~~138~~SIR intervals, ~~206,~~ and ~~316 keV, and the electron channels are 125, 183, 266, 396, 612, and 908 keV (from top to bottom~~ outside of ~~each panel, respectively, as the flux values decrease with increasing energy)~~either of these solar wind driver structures. The ~~field inclination panels show~~ chart shows the ~~results~~ number of individual teeth using the combined lists from ~~GOES magnetometers~~ CC09 and ~~LANL distribution function calculations and Tsyganenko (1989) model for $Kp = 2$ for reference~~this study.

Figure 5 shows an illustration of the relationship between the strength of driving to different modes of the magnetosphere. We compare quiet-time (AL > -100 nT), substorm (as identified from the list compiled in Ohtani and Gjerloev (2020)), storm (defined as 6-hour periods around peak Dst values below -75 nT), and sawtooth periods (from first to last sawtooth onset in

215 each sawtooth event) with their respective Dst, IMF B_z, solar wind speed, and AL responses. For each of the datasets, the

10

solid dot marks the mean of the values, while the ellipses are created using the standard deviation within each category. In this representation, sawtooth events are located in the "middle ground" between isolated substorms and full-scale geomagnetic storms Pulkkinen et al. (2007).
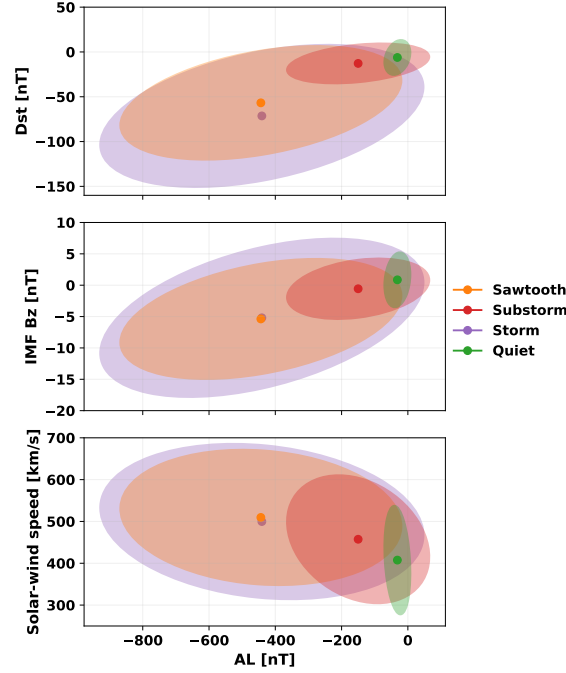

Figure 5. Modes of the magnetosphere with their drivers and responses. (top) Dst, (middle) IMF B_z, and (bottom) solar wind speed as function of the AL index. The solid dots show the mean in each category, with an ellipse created by the standard deviation of the distribution of values around the mean. Quiet time is defined as times where the AL index is greater than -100 nT. Substorms are defined as the time within 3 hours after onsets chosen by Ohtani and Gjerloev (2020). Storms are defined as times within 6 hours of Dst peak below -75 nT. Sawtooth intervals include times after the first sawtooth onset in the sequence to the last onset in the sequence.

To study the oxygen content in the inner magnetosphere associated with the sawtooth oscillations, RBSP-A and RBSP-B HOPE O^+ density was binned by L^* using $0.2L$-wide bins in the range $L^* = 1.5 - 6.0$, with median values computed over each half-orbit segment between rolling perigee/apogee to produce a contiguous time series per bin. For the sawtooth events, epoch time was selected to be the onset of the first tooth, and a superposed epoch analysis of the available HOPE observations was performed using SpacePy (Niehof et al., 2022) (left panels of Figure 6). For comparison, we performed a similar analysis using a list of storms identified as periods with minimum Dst below -75 nT, and storm onset identified from the start of the Dst decrease (right panels of Figure 6). The results for both are shown from -3 hours to $+48$ hours from epoch time.

Both STE onsets and storm onsets show a prompt inner magnetosphere O^+ density enhancement centered near $L^* \simeq 3 - 5$ that rises within a few hours of the epoch time ($t = 0$) and persists for tens of hours, with peak intensities of the order of 10^{-1} - 10^0 cm^{-3}. The enhancement is observed consistently by both spacecraft and span roughly $L^* \simeq 2.5 - 5.5$. The non-sawtooth
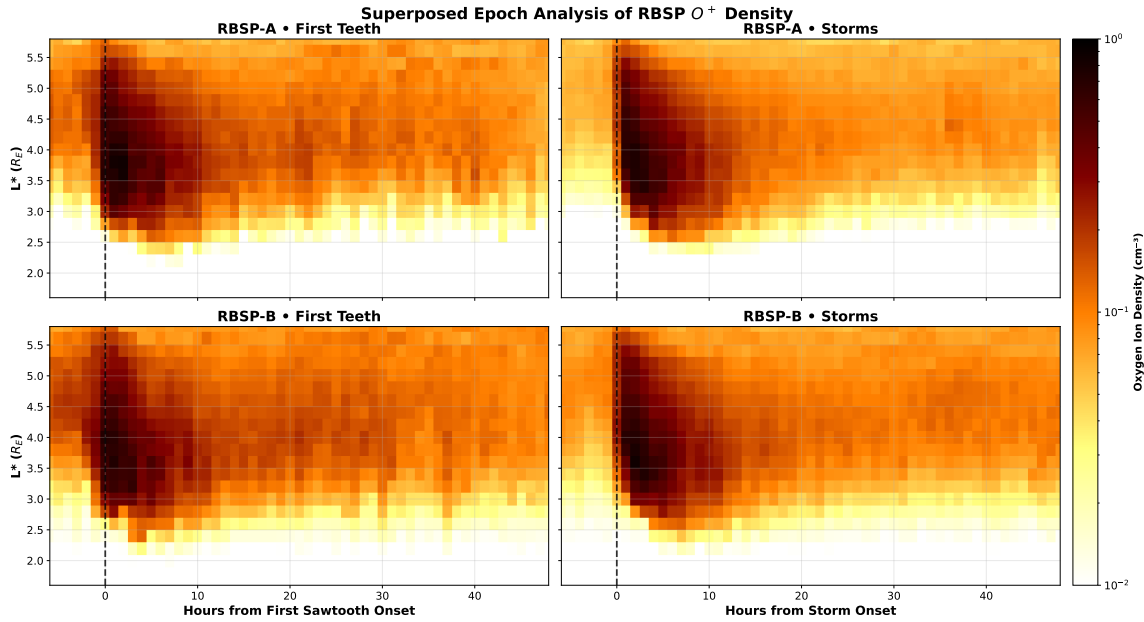
11

Figure 6. Superposed epoch analysis of RBSP-A and RBSP-B oxygen ion observations from the HOPE instrument. The x-axis represents time relative to epoch time. The observations are sorted into half-orbit bins and sorted relative to their L^* value. The timestamps represent the value at the center of the half-orbit. The oxygen number density is shown color coded in units of cm^{-3}.

storm results have similar radial extent and similar persistence to the sawtooth event results, and both categories share the same immediate post-onset increase and subsequent gradual decay toward pre-event levels over a time period of about 10-20 hours.

6 Discussion

In this study, we have identified sawtooth events using LANL energetic particle measurements from the period 2008 – 2016. ~~Comparing with prior~~ Analyzing this new statistic together with a prior list created by Cai and Clauer (2009) indicates that the characterizing properties of sawtooth oscillations, such as their recurrence intervals and the number of teeth per event, remain largely constant across the two solar cycles. This suggests that despite variations in solar wind conditions and geomagnetic activity, the underlying mechanisms governing sawtooth formation are robust.

Several open questions remain regarding the classification of sawtooth events and development of ~~a more objective~~ an objective (or programmable) definition of this phenomenon. Geomagnetic activity is often described by empirically defined modes including storms, sawtooth events, substorms, steady convection events and pseudobreakups in decreasing order of intensity. While the "typical best cases~~"~~" in each category have distinct features, there are overlaps and borderline cases that make ~~accurate distinction~~ unique identification challenging (Pulkkinen et al., 2010). However, even despite this overlap, the

magnetospheric processes during each of these modes are sufficiently different that they need to be separately addressed in order to fully understand the complexity of the solar wind–magnetosphere–ionosphere coupling.

~~Bracketed by individual substorms and magnetic storms, there still is no well-defined threshold for the level of solar wind driving or required magnetospheric or ionospheric conditions necessary to trigger or suppress sawtooth oscillations. It is also noteworthy to mention that the global MHD simulations~~ We identified STEs by visual inspection of multi-spacecraft geostationary proton flux, defining each tooth by the earliest onset across GEO; this is the same procedure used in prior catalogs such as Cai and Clauer (2009). Attempts to automate STE detection (fixed thresholds, template matching, clustering or machine learning classifiers) have not been ~~able to reproduce the sawtooth event signatures to good level of accuracy. Previous modeling studies suggest that periodic behavior can be recreated either with strong O^+ flux (Brambles et al., 2011), or with kinetic reconnection in~~ successful in reliable identification across the varying solar wind, solar cycle and magnetospheric conditions. This is likely because spacecraft local-time coverage varies and storm-time activity produces highly varying responses, yielding unacceptable false-positive and false-negative rates. Consequently, there is no validated automated alternative that would outperform conservative by-eye selection. Crucially, the STE phenomenology is visually distinctive – multi-MLT, quasi-periodic injections with repeatable sawtooth waveforms. Rigorous visual screening produces robust catalogs as evidenced by close agreement between independent lists in annual occurrence patterns, intertooth cadence, and teeth-per-event statistics despite different compilers and epochs. Lastly, we note that while there are many earlier works producing substorm lists based on algorithmic identification (Gjerloev, 2012; Frey et al., 2004; Forsyth et al., 2015; Juusola et al., 2011; Ohtani et al., 2020; McPherron, 202 , they do not yield consistent results, and the lists have at best ∼80% overlap even when based on the same input observations (e.g., the SML index). Rather than criticism of the ~~magnetotail (Wang et al., 2022).~~

~~The solar cycle dependence of sawtooth events shows that they predominantly occur during the declining phase of the solar cycle, with little increase in occurrence near solar maximum. This suggests the existence of a threshold beyond which stronger solar wind driving may suppress the periodic sawtooth oscillations, possibly transitioning the magnetosphere into a different, more disturbed and potentially more directly driven state. This result is consistent with previous work on magnetospheric modes (?Delzanno and Borovsky, 2022), which suggests that different levels of external driving can activate distinct large-scale responses in the system~~earlier studies, this fact should be treated as an indicator of the difficulty in quantitatively defining event sequences that originally were based on visual inspection of (multiple sources of) observations.

Using the LANL and GOES geostationary satellite datasets, we examined particle injections and magnetic field dipolarizations in different magnetic local time sectors (midnight, dawn, noon, dusk). Our analysis reveals that sawtooth events produce nearly simultaneous and almost similar intensity particle injections at all four MLT sectors, with higher dispersion patterns observed on the dayside. However, quantifying the exact level of dispersion remains difficult, as the satellite configurations vary from event to event, and the dispersion timings have to be done for each individual event and pair of spacecraft rather than examining the superposition which combines a range of conditions and configurations.

The superposed epoch analysis in Figure 3 highlights a key characteristic of sawtooth events: While energetic proton injections occur across all MLT sectors, significant magnetic field dipolarization is only observed in the midnight sector. This

suggests that the injections are a global phenomenon, likely driven by large-scale convection and tail reconnection, but the magnetic field ~~tilt~~ does not necessarily exhibit a corresponding global reconfiguration.

The absence of strong dipolarization in the noon, dawn, and dusk sectors indicates that the large-scale magnetic field structure remains relatively stable outside the midnight region. This finding challenges interpretations that sawtooth events involve a
280 system-wide restructuring of the magnetosphere. If large-scale dipolarization were the primary driver of sawtooth oscillations, we would expect synchronous dipolarization signatures at all MLT sectors. Instead, our findings support a scenario in which particle injections originate from nightside reconnection in a substorm-like manner, rather than from a global magnetospheric instability (Henderson, 2016).

The stretched field configuration shows a decrease and subsequent increase in the dawn and dusk plasma sheet before and
285 after onset. This pattern follows the expected diurnal variation, as a six-hour superposed epoch window captures the daily variation around the geostationary orbit. However, the night sector exhibits a clear dipolarization occurring approximately at the injection onset.

On the dayside, the magnetic configuration corresponds to the quiet time one before the injection onset, followed by a subsequent (minor) stretching of the magnetic field. This contradicts the idea that particle injections result from a compression-
290 driven inward transport of plasma from the dayside magnetopause. If magnetopause pressure pulses were responsible for inward particle transport, we would expect the dayside field to become compressed after onset, opposite to the observed effect. This finding further reinforces the idea that the sawtooth injection particles originate from periodic reconnection in the magnetotail transported by strongly enhanced convection.

Sawtooth occurrence is suppressed near solar maximum and elevated during the rising and declining phases of the solar cycle.
295 This pattern points to a driver threshold beyond which stronger, persistent forcing suppresses quasi-periodic cycling and shifts the system toward more directly driven stormtime responses. However, while interplanetary structures such as ICMEs peak during the declining solar cycle phase, there is not a one-to-one correspondence with the occurrence of ICMEs and sawtooth events. The long-term occurrence frequency pattern suggests that given levels of external driving activate different large-scale magnetospheric responses, rather than a linear mapping from solar wind driver structure to a magnetospheric response.

300 Sawtooth events can be classified by the intensity of the driver (solar wind speed, IMF B_z) or the state of the magnetosphere (average AL or Dst). In this classification, the sawtooth distribution resembles that of storms, but is more focused on moderate level of the driving solar wind/IMF as well as the storm intensity (Dst) or AL activity. These results suggest that rather than a given solar wind structure, the combination of intense but not extreme driver over an extended period is likely to lead to a sawtooth oscillation.

305 RBSP HOPE observations demonstrate a prompt O^+ density increase near $L^* \simeq 3-5$ following both first-tooth and storm onsets, with similar radial extent and persistence in both categories, implying that enhanced inner-magnetospheric oxygen accompanies onset but is not diagnostic of a unique "sawtooth driver" state (Figure 6). Together with the geostationary SEA showing global injections but midnight-localized dipolarization, these results support a reconnection-and-convection scenario in which magnetotail loading and preconditioning set onset thresholds and cadence, regardless of ion composition.

310 Earlier studies have shown that magnetotail reconnection can be enhanced by addition of heavy ions such as oxygen, as their

larger gyroradii allows them to demagnetize and thus decouple from the magnetic field at larger field values than the protons (Daglis, 2001; Kistler and Mouikis, 2016; Artemyev et al., 2020)

Taken together, the sawtooth oscillations are driven by conditions that often (but not always) are found during ICMEs or SIRs, and occur during geomagnetic storms and extended auroral electrojet activity. However sawtooth intervals are rarely if ever found during very high or extreme solar wind driving or geomagnetic activity, likely due to high driving and activity breaking the periodic onset sequence. Neither the driver characteristics (solar wind speed, IMF) nor the magnetospheric drivers (O^+ outflows) indicate periodicities that would lead to the roughly 180-minute intertooth interval. On the other hand, the period is very similar to substorm recurrence interval (Ohtani and Gjerloev, 2020; McPherron, 2023), which might point to an internal magnetospheric time scale for large-scale magnetotail reconnection event recurrence.

7 Conclusions

We have created a dataset of sawtooth events for solar cycle 24 that shows similar occurrence frequency characteristics to prior work from solar cycle 23. 23 (Cai and Clauer, 2009). Our superposed epoch analysis shows that the injections around the globe are near-simultaneous (global), but that the strong field dipolarizations is a repeatable feature only in the midnight sector (not global). The interval between the teeth in the event sequence is similar to values found for substorms both in observations and conceptual models (Borovsky and Yakymenko, 2017; Freeman and Morley, 2004). These results support a picture in which sawtooth events are created by magnetotail reconnection and very fast convection in the near-geostationary region.

Author contributions. C. DiMarco: Conceptualization, Methodology, Software, Analysis, Investigation, Data curation, Visualization, Writing—original draft, Writing and editing. T.I. Pulkkinen: Conceptualization, Methodology, Supervision, Writing and editing, Funding acquisition. M.G. Henderson: Data Resources, Supervision. All authors approved the final manuscript.

References

Angelopoulos, V., Sibeck, D., Carlson, C. W., McFadden, J. P., Larson, D., Lin, R. P., Bonnell, J. W., Mozer, F. S., Ergun, R., Cully, C., Glassmeier, K. H., Auster, U., Roux, A., LeContel, O., Frey, S., Phan, T., Mende, S., Frey, H., Donovan, E., Russell, C. T., Strangeway, R., Liu, J., Mann, I., Rae, J., Raeder, J., Li, X., Liu, W., Singer, H. J., Sergeev, V. A., Apatenkov, S., Parks, G., Fillingim, M., and Sigwarth, J.: First Results from the THEMIS Mission, in: The THEMIS Mission, edited by Burch, J. L. and Angelopoulos, V., pp. 453–476, Springer New York, New York, NY, ISBN 978-0-387-89819-3 978-0-387-89820-9, https://doi.org/10.1007/978-0-387-89820-9_19, 2009.

Artemyev, A. V., Angelopoulos, V., Runov, A., and Zhang, X.: Ionospheric Outflow During the Substorm Growth Phase: THEMIS Observations of Oxygen Ions at the Plasma Sheet Boundary, Journal of Geophysical Research Space Physics, 125, https://doi.org/https://doi.org/10.1029/2019ja027612, 2020.

Baker, D. N., Pulkkinen, T. I., Angelopoulos, V., Baumjohann, W., and McPherron, R. L.: Neutral line model of substorms: Past results and present view, Journal of Geophysical Research: Space Physics, 101, 12 975–13 010, https://doi.org/https://doi.org/10.1029/95ja03753, 1996.

Baker, D. N., Li, X., Pulkkinen, A., Ngwira, C. M., Mays, M. L., Galvin, A. B., and Simunac, K. D. C.: A major solar eruptive event in July 2012: Defining extreme space weather scenarios, Space Weather, 11, 585–591, https://doi.org/10.1002/swe.20097, _eprint: https://onlinelibrary.wiley.com/doi/pdf/10.1002/swe.20097, 2013.

Bame, S. J., McComas, D. J., Thomsen, M. F., Barraclough, B. L., Elphic, R. C., Glore, J. P., Gosling, J. T., Chavez, J. C., Evans, E. P., and Wymer, F. J.: Magnetospheric plasma analyzer for spacecraft with constrained resources, Review of Scientific Instruments, 64, 1026–1033, https://doi.org/10.1063/1.1144173, 1993.

Belian, R. D., Gisler, G. R., Cayton, T., and Christensen, R.: High-Zenergetic particles at geosynchronous orbit during the Great Solar Proton Event Series of October 1989, Journal of Geophysical Research, 97, 16 897, https://doi.org/10.1029/92ja01139, 1992.

Borovsky, J., Birn, J., and Ridley, A.: Unusual Solar Wind Associated with Global Sawtooth Oscillations: CCMC Simulations of the Magnetosphere, in: Living With a Star Workshop, https://lasp.colorado.edu/sdo/meetings/session_1_2_3/presentations/session3/3_09_Borovsky.pdf, 2004.

Borovsky, J. E. and Yakymenko, K.: Substorm occurrence rates, substorm recurrence times, and solar wind structure, Journal of Geophysical Research: Space Physics, 122, 2973–2998, https://doi.org/https://doi.org/10.1002/2016ja023625, 2017.

Borovsky, J. E., Lavraud, B., and Kuznetsova, M. M.: Polar cap potential saturation, dayside reconnection, and changes to the magnetosphere, Journal of Geophysical Research Atmospheres, 114, https://doi.org/https://doi.org/10.1029/2009ja014058, 2009.

Brambles, O. J., Lotko, W., Zhang, B., Wiltberger, M., Lyon, J., and Strangeway, R. J.: Magnetosphere Sawtooth Oscillations Induced by Ionospheric Outflow, Science, 332, 1183, https://doi.org/10.1126/science.1202869, 2011.

Brambles, O. J., Lotko, W., Zhang, B., Wiltberger, M., Lyon, J., and Strangeway, R. J.: Magnetosphere Sawtooth Oscillations Induced by Ionospheric Outflow, Science, 332, 1183, https://doi.org/10.1126/science.1202869, 2011.

Brambles, O. J., Lotko, W., Zhang, B., Ouellette, J., Lyon, J., and Wiltberger, M.: The effects of ionospheric outflow on ICME and SIR driven sawtooth events, Journal of Geophysical Research: Space Physics, 118, 6026–6041, https://doi.org/10.1002/jgra.50522, _eprint: https://onlinelibrary.wiley.com/doi/pdf/10.1002/jgra.50522, 2013.

Cai, X. and Clauer, C. R.: Investigation of the period of sawtooth events, Journal of Geophysical Research: Space Physics, 114, n/a–n/a, https://doi.org/10.1029/2008ja013764, 2009.

Cai, X., Zhang, J.-C., Clauer, C. R., and Liemohn, M. W.: Relationship between sawtooth events and magnetic storms, Journal of Geophysical Research: Space Physics, 116, n/a–n/a, https://doi.org/10.1029/2010ja016310, 2011.

380 Chen, Y., Cunningham, G., and Henderson, M.: Determination of errors in derived magnetic field directions in geosynchronous orbit: results from a statistical approach, Annales Geophysicae, 34, 831–843, https://doi.org/https://doi.org/10.5194/angeo-34-831-2016, 2016.

Daglis, I. A.: The storm-time ring current, Space Sci. Rev., 98, 343–363, 2001.

Delzanno, G. L. and Borovsky, J. E.: The Need for a System Science Approach to Global Magnetospheric Models, Frontiers in Astronomy and Space Sciences, 9, https://doi.org/https://doi.org/10.3389/fspas.2022.808629, 2022.

385 Forsyth, C., Rae, I. J., Coxon, J. C., Freeman, M. P., Jackman, C. M., Gjerloev, J., and Fazakerley, A. N.: A new technique for determining Substorm Onsets and Phases from Indices of the Electrojet (SOPHIE), Journal of Geophysical Research: Space Physics, 120, 10,592–10,606, https://doi.org/10.1002/2015JA021343, _eprint: https://agupubs.onlinelibrary.wiley.com/doi/pdf/10.1002/2015JA021343, 2015.

Freeman, M. P. and Morley, S. K.: A minimal substorm model that explains the observed statistical distribution of times between substorms, Geophysical Research Letters, 31, https://doi.org/https://doi.org/10.1029/2004gl019989, 2004.

390 Frey, H. U., Mende, S. B., Angelopoulos, V., and Donovan, E. F.: Substorm onset observations by IMAGE-FUV, Journal of Geophysical Research: Space Physics, 109, https://doi.org/10.1029/2004JA010607, _eprint: https://agupubs.onlinelibrary.wiley.com/doi/pdf/10.1029/2004JA010607, 2004.

Fung, S. F., Tepper, J. A., and Cai, X.: Magnetospheric state of sawtooth events, Journal of Geophysical Research: Space Physics, 121, 7860–7869, https://doi.org/10.1002/2016ja022693, 2016.

395 Funsten, H. O., Skoug, R. M., Guthrie, A. A., et al.: Helium, Oxygen, Proton, and Electron (HOPE) Mass Spectrometer for the Radiation Belt Storm Probes Mission, Space Science Reviews, 179, 423–484, https://doi.org/10.1007/s11214-013-9968-7, 2013.

Gjerloev, J. W.: The SuperMAG data processing technique, Journal of Geophysical Research: Space Physics, 117, n/a–n/a, https://doi.org/10.1029/2012ja017683, 2012.

Gonzalez, W. D., Joselyn, J. A., Kamide, Y., Kroehl, H. W., Rostoker, G., Tsurutani, B. T., and Vasyliunas, V. M.: What is a geomag-
400 netic storm?, Journal of Geophysical Research: Space Physics, 99, 5771–5792, https://doi.org/https://doi.org/10.1029/93JA02867, _eprint: https://agupubs.onlinelibrary.wiley.com/doi/pdf/10.1029/93JA02867, 1994.

Grandin, M., Aikio, A. T., and Kozlovsky, A.: Properties and Geoeffectiveness of Solar Wind High-Speed Streams and Stream Interaction Regions During Solar Cycles 23 and 24, Journal of Geophysical Research Space Physics, 124, 3871–3892, https://doi.org/https://doi.org/10.1029/2018ja026396, 2019.

405 Hajra, R. and Sunny, J. V.: Corotating Interaction Regions during Solar Cycle 24: A Study on Characteristics and Geoeffectiveness, Solar Physics, 297, https://doi.org/https://doi.org/10.1007/s11207-022-01962-1, 2022.

Heber, B., Sanderson, T., and Zhang, M.: Corotating interaction regions, Advances in Space Research, 23, 567–579, https://doi.org/https://doi.org/10.1016/s0273-1177(99)80013-1, 1999.

Henderson, M. G.: Recurrent embedded substorms during the 19 October 1998 GEM storm, Journal of Geophysical Research: Space Physics,
410 121, 7847–7859, https://doi.org/https://doi.org/10.1002/2015JA022014, 2016.

Henderson, M. G., Reeves, G. D., Skoug, R., Thomsen, M. F., Denton, M. H., Mende, S. B., Immel, T. J., Brandt, P. C., and Singer, H. J.: Magnetospheric and auroral activity during the 18 April 2002 sawtooth event, Journal of Geophysical Research, 111, https://doi.org/10.1029/2005ja011111, 2006.

Juusola, L., Østgaard, N., Tanskanen, E., Partamies, N., and Snekvik, K.: Earthward plasma sheet flows during sub-storm phases, Journal of Geophysical Research: Space Physics, 116, https://doi.org/10.1029/2011JA016852, _eprint: https://onlinelibrary.wiley.com/doi/pdf/10.1029/2011JA016852, 2011.

Kilpua, E., Koskinen, H. E. J., and Pulkkinen, T. I.: Coronal mass ejections and their sheath regions in interplanetary space, Living Reviews in Solar Physics, 14, 5, https://doi.org/10.1007/s41116-017-0009-6, 2017a.

Kilpua, E. K. J., O, L. C., G, L. J., and Li, Y.: Interplanetary coronal mass ejections in the near-Earth solar wind during the minimum periods following solar cycles 22 and 23, Annales Geophysicae, 29, 1455–1467, https://doi.org/https://doi.org/10.5194/angeo-29-1455-2011, 2011.

Kilpua, E. K. J., Balogh, A., von Steiger, R., and Liu, Y. D.: Geoeffective Properties of Solar Transients and Stream Interaction Regions, Space Science Reviews, 212, 1271–1314, https://doi.org/10.1007/s11214-017-0411-3, 2017b.

Kistler, L. M. and Mouikis, C. G.: The inner magnetosphere ion composition and local time distribution over a solar cycle, Journal of Geophysical Research: Space Physics, 121, 2009–2032, https://doi.org/https://doi.org/10.1002/2015ja021883, 2016.

Lee, D., Lyons, L. R., Kim, K. C., Baek, J., Kim, K., Kim, H., Weygand, J., Moon, Y., Cho, K., Park, Y. D., and Han, W.: Repetitive substorms caused by Alfvénic waves of the interplanetary magnetic field during high-speed solar wind streams, Journal of Geophysical Research Atmospheres, 111, https://doi.org/https://doi.org/10.1029/2006ja011685, 2006.

Lee, D.-Y.: Sawtooth oscillations directly driven by solar wind dynamic pressure enhancements, Journal of Geophysical Research, 109, https://doi.org/10.1029/2003ja010246, 2004.

McPherron, R. L.: Substorm Triggering by the Solar Wind, Journal of Geophysical Research: Space Physics, 128, e2022JA031 147, https://doi.org/10.1029/2022JA031147, _eprint: https://agupubs.onlinelibrary.wiley.com/doi/pdf/10.1029/2022JA031147, 2023.

NASA Goddard Space Flight Center: Space Physics Data Facility, https://spdf.gsfc.nasa.gov/, 2025.

Niehof, J. T., Morley, S. K., Welling, D. T., and Larsen, B. A.: The SpacePy space science package at 12 years, Frontiers in Astronomy and Space Sciences, 9, https://doi.org/10.3389/fspas.2022.1023612, 2022.

Nowrouzi, N., Kistler, L. M., Zhao, K., Lund, E. J., Mouikis, C., Payne, G., and Klecker, B.: Differences in Ionospheric O+ and H+ Outflow During Storms With and Without Sawtooth Oscillations, Geophysical Research Letters, 51, https://doi.org/https://doi.org/10.1029/2024gl109551, 2024.

Ohtani, S. and Gjerloev, J. W.: Is the Substorm Current Wedge an Ensemble of Wedgelets?: Revisit to Midlatitude Positive Bays, Journal of Geophysical Research Space Physics, 125, https://doi.org/https://doi.org/10.1029/2020ja027902, 2020.

Ohtani, S., Motoba, T., Takahashi, K., and Califf, S.: Generalized Substorm Current Wedge Model: Two Types of Dipolarizations in the Inner Magnetosphere, Journal of Geophysical Research: Space Physics, 125, e2020JA027 890, https://doi.org/10.1029/2020JA027890, _eprint: https://onlinelibrary.wiley.com/doi/pdf/10.1029/2020JA027890, 2020.

Papitashvili, N., Bilitza, D., and King, J.: OMNI: A Description of Near-Earth Solar Wind Environment, in: 40th COSPAR Scientific Assembly, 2-10 August, 2014, Moscow, Russia, vol. 40, pp. C0.1–12–14, 2014.

Partamies, N., Pulkkinen, T. I., McPherron, R. L., McWilliams, K., Bryant, C. R., Tanskanen, E., Singer, H. J., Reeves, G. D., and Thomsen, M. F.: Different magnetospheric modes: solar wind driving and coupling efficiency, Annales Geophysicae, 27, 4281–4291, 2009.

Pulkkinen, T. I., Ganushkina, N. Y., Tanskanen, E. I., Kubyshkina, M., Reeves, G. D., Thomsen, M. F., Russell, C. T., Singer, H. J., Slavin, J. A., and Gjerloev, J.: Magnetospheric current systems during stormtime sawtooth events, Journal of Geophysical Research: Space Physics, 111, https://doi.org/https://doi.org/10.1029/2006ja011627, 2006.

19

Pulkkinen, T. I., Partamies, N., McPherron, R. L., Henderson, M., Reeves, G. D., Thomsen, M. F., and Singer, H. J.: Comparative statistical analysis of storm time activations and sawtooth events, Journal of Geophysical Research: Space Physics, 112, n/a–n/a, https://doi.org/10.1029/2006ja012024, 2007.

Pulkkinen, T. I., Palmroth, M., Koskinen, H. E. J., Laitinen, T. V., Goodrich, C. C., Merkin, V. G., and Lyon, J. G.: Magnetospheric modes and solar wind energy coupling efficiency, Journal of Geophysical Research, 115, 2010.

Richardson, I. G. and Cane, H. V.: Near-Earth Interplanetary Coronal Mass Ejections During Solar Cycle 23 (1996 - 2009): Catalog and Summary of Properties, Solar Physics, 264, 189–237, https://doi.org/10.1007/s11207-010-9568-6, 2010.

Sergeev, V. A., Pellinen, R. J., and Pulkkinen, T. I.: Steady magnetospheric convection: A review of recent results, Space Science Reviews, 75, 551–604, 1996.

Singer, H. J., Matheson, L., Grubb, R., Newman, A., and Bouwer, S. D.: Monitoring Space Weather with the GOES Magnetometers, in: SPIE Conference Proceedings, GOES-8 and Beyond, edited by Washwell, E. R., vol. 2812, pp. 299–308, 1996.

Spence, H. E., Reeves, G. D., Baker, D. N., et al.: Science goals and overview of the Radiation Belt Storm Probes (RBSP) Energetic Particle, Composition, and Thermal Plasma (ECT) suite on NASA's Van Allen Probes, Space Science Reviews, 179, 311–336, https://doi.org/10.1007/s11214-012-9908-y, 2013.

Thomsen, M. F., McComas, D. J., Reeves, G. D., and Weiss, L. A.: An observational test of the Tsyganenko (T89a) model of the magnetospheric field, Journal of Geophysical Research: Space Physics, 101, 24 827–24 836, https://doi.org/https://doi.org/10.1029/96ja02318, 1996.

Tsyganenko, N.: A magnetospheric magnetic field model with a warped tail current sheet, Planetary and Space Science, 37, 5–20, https://doi.org/https://doi.org/10.1016/0032-0633(89)90066-4, 1989.

Wang, X., Chen, Y., and Tóth, G.: Simulation of Magnetospheric Sawtooth Oscillations: The Role of Kinetic Reconnection in the Magnetotail, Geophysical Research Letters, 49, https://doi.org/10.1029/2022gl099638, 2022.